ACS OMEGA

Open Access

http://pubs.acs.org/journal/acsodf

Article

An RNA Helicase DHX33 Inhibitor Shows Broad Anticancer Activity via Inducing Ferroptosis in Cancer Cells

Xiyu Tang,[#] Yuanlian Deng,[#] Yingying Liang,[#] Deqing Liao, Fuyu Wen, and Yandong Zhang*

Cite This: *ACS Omega* 2024, 9, 28372−28384

Read Online

ACCESS | Metrics & More | Article Recommendations | Supporting Information

ABSTRACT: RNA helicase DHX33 has been identified as a critical factor promoting cancer development. In the present study, a previously developed small molecule inhibitor for DHX33, KY386, was found to robustly kill cancer cells via a new path, the ferroptosis pathway. Mechanistically, DHX33 promotes the expression of critical players in lipid metabolism including FADS1, FADS2, and SCD1 genes, thereby sensitizing cancer cells to ferroptosis mediated cell death. Our study reveals a novel mechanism of DHX33 in promoting tumorigenesis and highlights that pharmacological targeting DHX33 can be a feasible option in human cancers. Normally differentiated cells are insensitive to DHX33 inhibition, and DHX33 inhibitors have little cellular toxicity in vitro and in vivo. Our studies demonstrated that DHX33 inhibitors can be promising anticancer agents with great potential for cancer treatment.

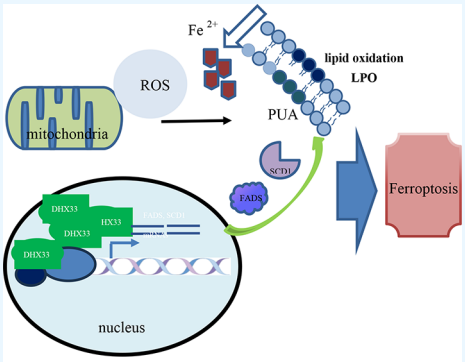

INTRODUCTION

Helicases can be divided into DNA and RNA helicases based on their activities toward DNA or RNA molecules.[1] RNA helicases are modulators of RNA structures, and they play critical roles in all aspects of RNA metabolism.[2,3] DEAD/DEAH box proteins constitute one of the largest subfamily of RNA helicases, these proteins share eight distinct peptide motifs in their primary structures, and one of them is a DEAD/DEAH motif.[2] These conserved motifs are located primarily in the helicase core and involved in substrate binding and ATP/NTP hydrolysis.[4]

Most RNA helicases are large proteins containing multiple domains, which allow the binding of cofactors to influence their activity in cells in a spacial and temporal manner.[5] Therefore, most RNA helicases form protein complexes such as RNP complexes or DNA/RNA-protein complexes to exert their functions.[6] Specific protein cofactors in the RNA helicase complex help RNA helicases to recognize different substrates in cells and therefore modulate different cellular activities.[7] Different protein cofactors influence different RNA helicase functions or activities.[8]

Most RNA helicases have two enzymatic activities which are coupled, the ATPase and helicase activities.[9−11] The ATPase reaction core of many RNA helicases highly resemble one another, while the helicase core is different from one RNA helicase to another.[5] Development of inhibitors that are specific for a single RNA helicase is feasible, as long as the inhibitors avoid targeting helicase common sites.

RNA helicases can be abnormally expressed under different pathological conditions.[12] Due to their important roles in gene regulation and cellular activities, helicases have been considered as treatment targets for human diseases.[6,13] DHX33 has been found to play diverse roles in ribosome biogenesis, cell proliferation, apoptosis, cell migration, innate immunity, and adaptive immunity.[14−18] Additionally, DHX33 protein has been found to be overexpressed in a few types of human cancers.[15,19−22] Previous results indicate that DHX33 regulates the transcription of a subset of genes in diverse cancer related pathways such as glucose metabolism, cytokinesis, apoptosis, DNA architecture, and cell migration.[16,23−26]

We have previously developed a highly potent inhibitor of DHX33, KY386, with a moderate pharmacokinetic property and metabolic stability.[27] In this study, KY386 is found to efficiently reduce the growth of various human cancer cell lines and organoids and demonstrated to have an efficient cancer inhibitory effect in various human cancer xenografts with little toxicity in vivo.

Ferroptosis is a new form of cell death initially discovered in 2012.[28] There are several hallmarks for this type of cell death, one of them is higher ROS levels which may be caused by environmental or intracellular factors, and another hallmark is the unrestrained lipid peroxidation that is Fe^{2+} dependent.[28,29] Polyunsaturated fatty acid (PUFA) plays a central role in the induction of ferroptosis, as they are the precursors of lipid

Received: March 7, 2024
Revised: June 3, 2024
Accepted: June 5, 2024
Published: June 17, 2024

peroxide (LPO).[30] Cancer cells with higher levels of PUFA are sensitized to ferroptosis.[31] As redox levels in cells are tightly correlated to the induction of ferroptosis, several important players in regulating GSH levels, GPX4, SLC3A2, and SCL7A11 are critical players in ferroptosis.[32−34] Additionally, several enzymes involved in fatty acid synthesis such as stearoyl CoA desaturase (SCD)-1 and fatty acid desaturases (FADS1 and FADS2), play important roles in the synthesis of PUFAs.[35] Therefore, cancer cells with higher levels of SCD1 and FADS1/FADS2 are prone to undergo ferroptosis.[36−38]

In this study, KY386 was found to robustly kill cancer cells via ferroptosis. Cancer cells that were treated with KY386 have much higher levels of reactive oxygen species (ROS), Fe^{2+}, and LPO, and much lower levels of glutathione (GSH), which are consistent with ferroptosis characteristics.

MATERIALS AND METHODS

Cell Culture. DU145, HCT-116, HepG2, K-562, MIA PaCa-2, PC-3, SK-BR-3, NCI-H1299, NCI-H1975, HCC1806, SNU-1, BT549, U-937, HCT-15, A-498, A549, Daudi, Jurkat T, U-118MG, SNU-387, Caki-1, SNU-423, COLO829, KATO-III, Capan-1, Malme-3M, HeLa, U-87MG, Hep 3B, and HEK293T cell lines were purchased from ATCC. LoVo, LS180, SW480, CALU-1, T84, and SK-HEP-1 were purchased from ECACC. KYSE-150 was purchased from DSMZ. HuH-7 was purchased from JCRB. NCI-N87, MeWo, HEEC, HGC27 HSF, and A375 and SGC7901 cell lines were purchased from Shanghai Cell Bank.

DU145, HCT-116, HepG2, K-562, LoVo, MDA-MB-231, MIA PaCa-2, PC-3, SK-BR-3, NCI-H1299, NCI-H1975, HCC1806, SNU-1, BT549, HCT-15, U-937, A-498, KYSE-150, A549, Daudi, Jurkat T, SNU-387, SW480, Caki-1, SNU-423, CALU-1, COLO 829, T84, U-87MG, NCI-N87, MeWo, HEEC, HGC27 and SGC7901 cells were cultured in an RPMI 1640 medium supplemented with 10% FBS and 1% P/S (penicillin and streptomycin, 100 units/mL) at 37 °C under a humidified atmosphere of 95% air and 5% CO_2. LS180, Hep 3B, and SK-HEP-1 cells were cultured in an EMEM medium supplemented with 10% FBS, 2 mM glutamine, 1% NEAA, and 1% P/S (penicillin and streptomycin, 100 units/mL) at 37 °C under a humidified atmosphere of 95% air and 5% CO_2. HuH-7, U-118MG, HSF, HEK293T, and A375 cells were cultured in DMEM supplemented with 10% FBS and 1% P/S (penicillin and streptomycin, 100 units/mL) at 37 °C under a humidified atmosphere of 95% air and 5% CO_2. KATO-III, Capan-1, and Malme-3 M cells were cultured in the IMDM medium supplemented with 20% FBS and 1% P/S (penicillin and streptomycin, 100 units/mL) at 37 °C under a humidified atmosphere of 95% air and 5% CO_2. HeLa cells were cultured in an L-15 medium supplemented with 10% FBS and 1% P/S (penicillin and streptomycin, 100 units/mL) at 37 °C under a humidified atmosphere of 100% air. MEF cells were isolated as described previously and maintained in DMEM medium containing 10% fetal bovine serum (FBS), 2 mM L-glutamine, and streptomycin and penicillin.[39] A875 and AN3CA cells were purchased from ATCC and cultured in MEM supplemented with 10% fetal bovine serum (FBS), nonessential amino acids, 2 mML-glutamine, streptomycin, and penicillin. HEC-1A cells were purchased from Shanghai Cell Bank and cultured in a McCoy 5A medium supplemented with 10% FBS and penicillin−streptomycin. All cells were maintained in a CO_2 incubator at 37 °C with humidity.

CTG Experiment. For adherent cells, the culture medium was removed from the culture flask, and then 10 mL of DPBS was used to wash cells once. 3 or 2 mL of 0.25% trypsin−EDTA solution was added into a T150 or T75 flask to detach the cells by incubating at 37 °C for 3−5 min. 10 mL of the complete medium (with FBS) was added to stop the digestion, and cells were resuspended by pipetting up-and-down using a serological pipet for several times. Cells were then analyzed on a Vi-CellXR automated cell counter. Cells were diluted to an appropriate density, a reservoir of cell suspension was prepared, and 90 μL of cell suspension (containing about 2000−8000 cells total) was dispensed into each well into a 96-well plate. The cells were cultured overnight at 37 °C. For suspension cells, cell clumps, if any, were broken by pipetting cells up-and-down several times. A cell reservoir was prepared for each cell line and dispensed into a 96-well assay plate as describe above. The cells were cultured overnight at 37 °C. The next day, the intermediate compound plate was prepared, and 10 μL of the culture medium containing 10X compounds (KY386) was added using a multichannel pipet into respective wells on the 96-well cell plates. A medium containing only DMSO (0.05%, v/v) was used as the negative control in the assay. Cells were incubated with the compounds for 72 h at 37 °C. At the end of compound treatment, ATP content in each well, which serves as a surrogate of cell viability, was measured by using the CellTiter-Glo (Promega) reagent. 100 μL of the 2X CellTiter-Glo buffer was added into each well of a 96-well plate using a Multidrop liquid dispenser with gentle shaking. The cell plate was centrifuged at 200 × g for 1 min. The plate was incubated for 15 min, and then luminescence signals were recorded on an Envision plate reader. Cell viability was analyzed using luminescence values.

Lentivirus Production. To produce lentivirus, pLKO.1-shRNA and virus packaging plasmid pCMV-VSV-G and pCMV$_\triangle$R8.2 were transfected into HEK293T cells with the Lipofectamine 2000 reagent (Life Technologies). The shRNA sequence targeting human DHX33 has been described previously.[40] 48 h later, the culture supernatant was collected and centrifuged at 2000 rpm for 2 min. Virus was then aliquoted and frozen at −80 °C.

CCK-8 Analysis. CCK-8 (Yeasen Biotechnology (Shanghai)) analysis was used to evaluate the viability of cells according to the standard protocol from the manufacturer's recommendations.

Apoptosis Analysis. Apoptosis assay was performed with a Vybrant apoptosis kit #2 (Molecular Probes) according to the manufacturer's protocol.

Soft Agar Assay. Depending on different cell types, cells were plated into complete growth media supplemented with agar to support three-dimentional growth. Generally, 1.0×10^4 cells were mixed in 4.0 mL of 0.3% agar/media/10% FBS as the top agar and plated into 60 mm plates with 4.0 mL of 0.6% agar/media/10% FBS as the base agar. Plates were incubated at 37 °C, checked every 3 days, and fed with 2.0 mL of 0.3% agar/media/10% FBS every week. Colonies were photographed and counted 2−3 weeks later.

Western Blot. Cells were lysed by RIPA buffer supplemented with protease and phosphatase inhibitors (Thermo Fisher). After incubation for 10 min on ice, cell lysates were further disrupted by sonication. The whole cell extract was then subjected to a SDS-PAGE gel with a loading amount of 50 μg of protein per sample. Proteins were then transferred onto a polyvinylidene difluoride membrane.

https://doi.org/10.1021/acsomega.4c02265
ACS Omega 2024, 9, 28372−28384

Membranes were blocked in 5% nonfat milk which was diluted in 1X TBST buffer for 1 h at room temperature. Primary antibodies that were diluted in 5% FBS (diluted in 1X TBST) were incubated with the membrane at 4 °C overnight. Membranes were then rinsed with 1X TBST buffer multiple times and incubated with HRP-labeled secondary antibodies in 5% FBS (diluted in 1X TBST) at room temperature for 2 h. Blots are visualized with an ECL kit (Thermo fisher). The antibodies were sourced as follows: anti-GAPDH, Absin (abs830030); anti-DHX33, Bethyl (A300−800A); anti-DHX33, Santa Cruz Biotechnology (B-4, sc-390573); anti-FADS1, ABclonal (A0178); anti-FADS2, ABclonal (A10270); anti-SCD1, ABclonal (A16429); anti-SLC7A11, ABclonal (A13685); anti-SCL3A2, Solarbio (K007294P); anti-GPX4, Beyotime (AF7020).

Quantitative Real-Time PCR. The primers were all designed by IDT (http://sg.idtdna.com/site) as an online "realtime PCR tool" and purchased from BGI (Shenzhen). Total RNA was extracted using a high pure RNA isolation kit (Roche) and then transcribed into cDNA using a PrimeScript mix kit (Takara). Real-time PCR is performed with an ABI One step plus cycler that is managed with the corresponding software. To analyze mRNA levels, SYBR green supermix (Bio-Rad) was used, and transcript quantification was calculated usign the $\triangle\triangle$CT value after normalized to GAPDH or histone H3.3 values. The melting curve was used to confirm the amplification of a single product. All primer sequences for this study are shown below (all primers start from 5′ to 3′):

H3.3-Forward TGTGGCGCTCCGTGAAATTAG
H3.3-Reverse CTGCAAAGCACCGATAGCTG
SCD-Forward CCTGGTTTCACTTGGAGCTGTG
SCD-Reverse TGTGGTGAAGTTGATGTGCCAGC
FADS1-Forward CTGTCGGTCTTCAGCACCTCAA
FADS1-Reverse CTGGGTCTTTGCGGAAGCAGTT
FADS2-Forward TGCAACGTGGAGCAGTCCTTCT
FADS2-Reverse GGCACATAGAGACTTCACCAGC
SLC7A11-Forward GGAGAAGGAATTCCAGGTCAT
SLC7A11-Reverse ATGGTGGACACAACAGGCTT
GPX4-Forward AGAGATCAAAGAGTTCGCCGC
GPX4-Reverse TCTTCATCCACTTCCACAGCG

ROS Detection. Intracellular ROS levels were analyzed using a Reactive Oxygen Species (ROS) Fluorometric Assay Kit (Elabscience) according to the manufacturer's instructions. After drug treatment for 16h, the cells were treated with the reagent DCFH-DA, which would be converted into a fluorescent substance DCF. DCF could not penetrate the cell membrane, and the emission signal at 530 nm would be recorded using a multifunctional plate reader (Nivo, PerkinElmer).

LPO Detection. Drug-treated cells were harvested after centrifugation at a low speed (4 °C, 1000 rpm) for 10 min. A volume of 300−500 μL of PBS (pH 7.4) was added to resuspend the cells. The cells were then disrupted by ultrasonication, and the supernatant was collected after centrifugation. LPO analysis was analyzed using a LPO detection kit (Elabscience) based on the manufacturer's recommendation.

Fe^{2+} Detection. Drug-treated cells were harvested after trypsin treatment. Approximately 10^6 cells in each sample were suspended in 200 μL of lysis buffer and sonicated for lysis. The supernatant was collected after centrifugation at 15 000 × g for 10 min. The Fe^{2+} levels in cells were analyzed using a Cell Ferrous Iron Colorimetric Assay Kit (Elabscience) according to the manufacturer's recommendation.

GSH Detection. Drug-treated cells were harvested, washed once in PBS, and lysed in 1% Triton X100 buffer. The GSH content was determined using a Reduced Glutathione (GSH) Colorimetric Assay Kit (Elabscience) following the manufacturer's recommendation.

Compound Inhibitory Test in Human Cancer Organoids. Human cancer organoids with the Ras G12 V or Ras G12D mutation were purchased from Beijing K2 Oncology Medical Technology Co., Ltd. The detailed pathological information is shown in Table S1. Right after thawing from the liquid nitrogen tank, cells were diluted with 5 mL of Advance DMEM containing 10% FBS. After centrifugation at 300 × g for 5 min, the cell pellet was resuspended with the GAS-Ad-ES medium (X), and a cold matrigel was then added and mixed well. Cells were then seeded into 24-well plates and put in a CO_2 incubator at 37 °C for 30 min. The GAS-Ad-ES medium was then added, and cells were further incubated for 1 week. Cells were fed with a fresh medium every 3 days. For the drug potency test, cells were digested by trypsin and then resuspended in the GAS-Ad-ES medium. Cell concentration was adjusted to 1.6×10^5 cells/ml. The matrigel was thawed at 4 °C and then mixed with the cell suspension; 50 μl of the mixture was then pipetted into a 96-well plate and then incubated at 37 °C for 30 min; the GAS-Ad-ES medium was then added, and cells were further incubated for 2 days. Drugs at different concentrations were then added into the wells, and cancer organoids were treated for 5 days. Cell viability was examined after 50 μL of LCTG solution was added at each well at the end point. Plates were read 5−10 min later based on chemiluminescence. DMSO was used as a negative control, while 2.5 μM BEZ235 was used as a positive control.

Mouse Xenograft Model (Cell Line Derived Xenograft). All mouse experiments followed the standard guidelines. Nude female mice were purchased from Beijing Vital River and received standard institutional care. Cancer cells were trypsinized and resuspended with PBS at a final concentration of 1×10^8 cells/mL. Five-week old Nude mice were subjected to subcutaneous injection with 1×10^7 cells along their flank. When tumors reached to a size of approximately 150 mm^3 in the tumor volume, mice were grouped randomly, and drugs were administrated through intraperitoneal injection. The DHX33 inhibitor (free base) was formulated in 10% PEG400, 5% Cremophor ELP, 2.5% Tween-80, and 82.5% deionized aqueous solution, administrated at the indicated doses for IP injections, BID or TID.

Patient Derived Xenograft (PDX Model). Patient tumor tissues were thawed from a liquid nitrogen tank at 37 °C in a water bath. Tumor tissues were then sliced into $2 \times 2 \times 3$ mm^3 pieces and put into RPMI 1640 complete media for use. Nude mice of age 8 week old were euthanized, and tumor slices were then inoculated with 11G cannula needle subcutaneously at the right flank. Well grown tumor tissues were selected for further dissection, connective tissues and necrotic tissues were removed, tumor tissues were further sliced into $2 \times 2 \times 2$ mm^3 pieces and inoculated into nude mice subcutaneously. When tumor tissues grew into an average volume of 150 mm^3, mice were randomly grouped into the vehicle control and experimental group. The DHX33 inhibitor was formulated in 10% PEG400, 5% Cremophor ELP, 2.5% Tween-80, and 82.5% deionized aqueous solution, administrated at the indicated doses for IP injections, BID or TID.

https://doi.org/10.1021/acsomega.4c02265
ACS Omega 2024, 9, 28372−28384

A

Cell type	Cell line	KY386 CC_{50}(μM)		
		1st exp.	2nd exp.	3rd exp.
Liver cancer	HepG2	0.0559	0.0673	0.0827
	SK-HEP-1	0.0602	0.0499	0.077
	HuH-7	0.0547	0.0511	0.0548
	Hep3B	1.471	2.123	1.043
	SNU-387	0.0427	0.0452	0.0428
	SNU-423	0.0698	0.0821	0.0613
Lung cancer	A549	0.0445	0.0418	0.0463
	Calu-1	*>10	0.5045	0.1432
	NCI-H1299	0.0362	0.0309	0.0352
	NCI-H1975	0.0763	0.0654	0.0647
Pancreatic cancer	Mia-pa-ca-2	0.0669	0.0805	0.0976
	Capan-1	*>10	*>10	*>10
Colorectal cancer	HCT116	0.0419	0.0521	0.0553
	HCT-15	0.0308	0.0346	0.0291
	LoVo	0.0563	0.0594	0.0991
	LS 180	0.0866	0.0799	0.085
	SW 480	0.2948	0.3918	0.3594
	T84	0.0453	0.0461	0.044
Gastric cancer	KATO-III	0.071	0.0733	0.076
	SNU-1	0.08	0.0648	0.0938
Breast cancer	BT-549	0.0538	0.05	0.0536
	HCC1806	0.0408	0.0331	0.0338
	MDA-MB-231	0.0857	0.0961	0.1009
	SK-BR-3	0.0427	0.047	0.0448
Leukemia	Daudi	0.0741	0.0638	0.0705
	Jurkat	0.0465	0.0333	0.0402
	K562(3K cell)	0.0319	0.0322	0.0427
	U-937	0.0242	0.0244	0.0369
Renal cancer	A-498	0.0409	0.0434	0.0393
	Caki-1	0.0421	0.0497	0.0526
Prostate cancer	DU145	0.0673	0.0685	0.0712
	PC-3	0.0428	0.0563	0.0464
Esophageal Cancer	KYSE-150	0.0515	0.0628	0.056
Cervical cancer	Hela	0.0928	0.0978	0.0603
Brain cancer	U-118 MG	0.0365	0.05	0.0438
	U-87MG	0.0801	0.079	0.0752
Melanoma	COLO 829	*>10	*>10	*>10
	Malme-3M	0.0699	0.0574	0.0487

B

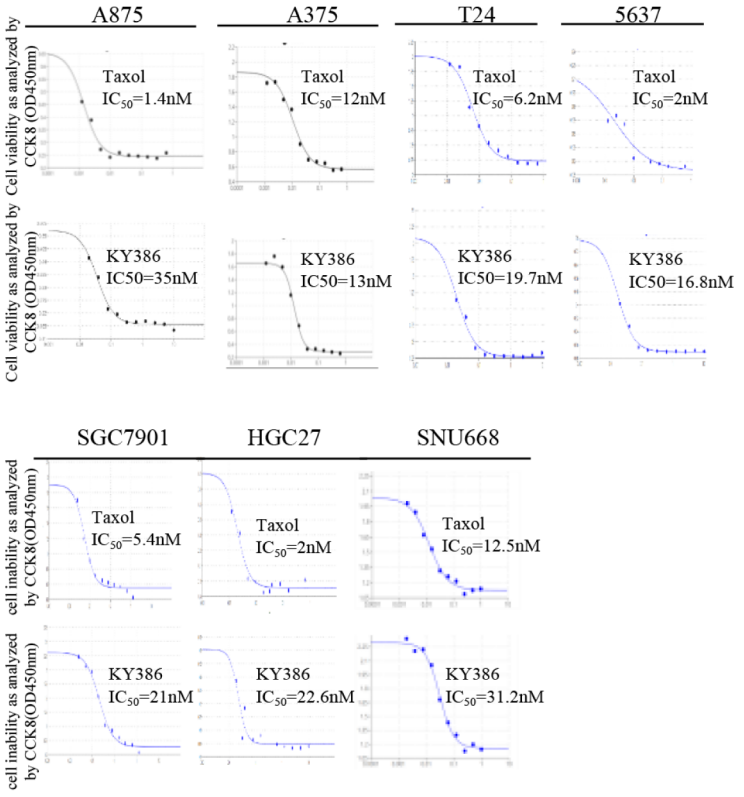

C

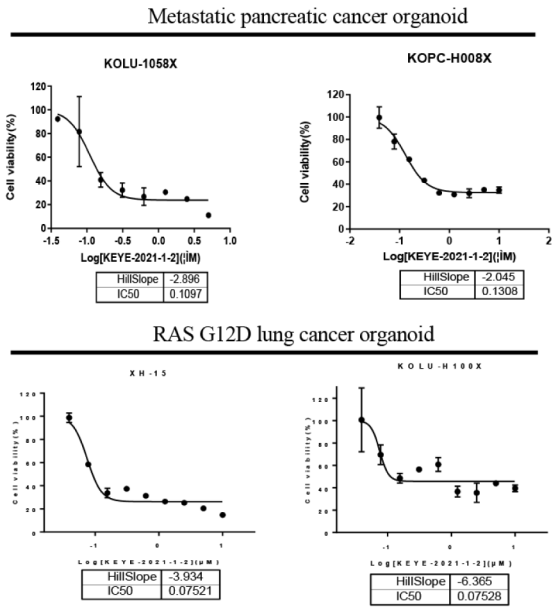

Figure 1. KY386 shows broad anticancer activity. A. 38 different cancer cell lines were treated with KY386 at multiple doses for 72 h, and ATP content was measured and used as a surrogate of cell viability using the CellTiter-Glo assay. Three independent experiments were repeated, and each individual IC_{50} was listed in the table. B. CCK-8 analysis was performed on the designated cancer cell lines for KY386 efficacy in vitro. Cells were treated at multiple doses for 72 h. Taxol was used as a positive control for comparison. The calculated IC_{50} was labeled in the graph. C. Three human cancer organoids, each of metastatic pancreatic cancer and lung cancer with RAS gene mutation (G12 V or G12D) were used for the KY386 drug potency test. Cell viability was plotted against the concentration of KY386 (in log values). IC_{50} was calculated and shown.

Statistical Analysis. Data are presented as the mean ± SD. Statistical significance was determined using Student's *t* test, with a *p* value <0.05 considered significant. *, $p < 0.05$; **, $p < 0.01$; ***, $p < 0.001$; ****, $p < 0.0001$, $n = 3$ if not specified.

https://doi.org/10.1021/acsomega.4c02265
ACS Omega 2024, 9, 28372−28384

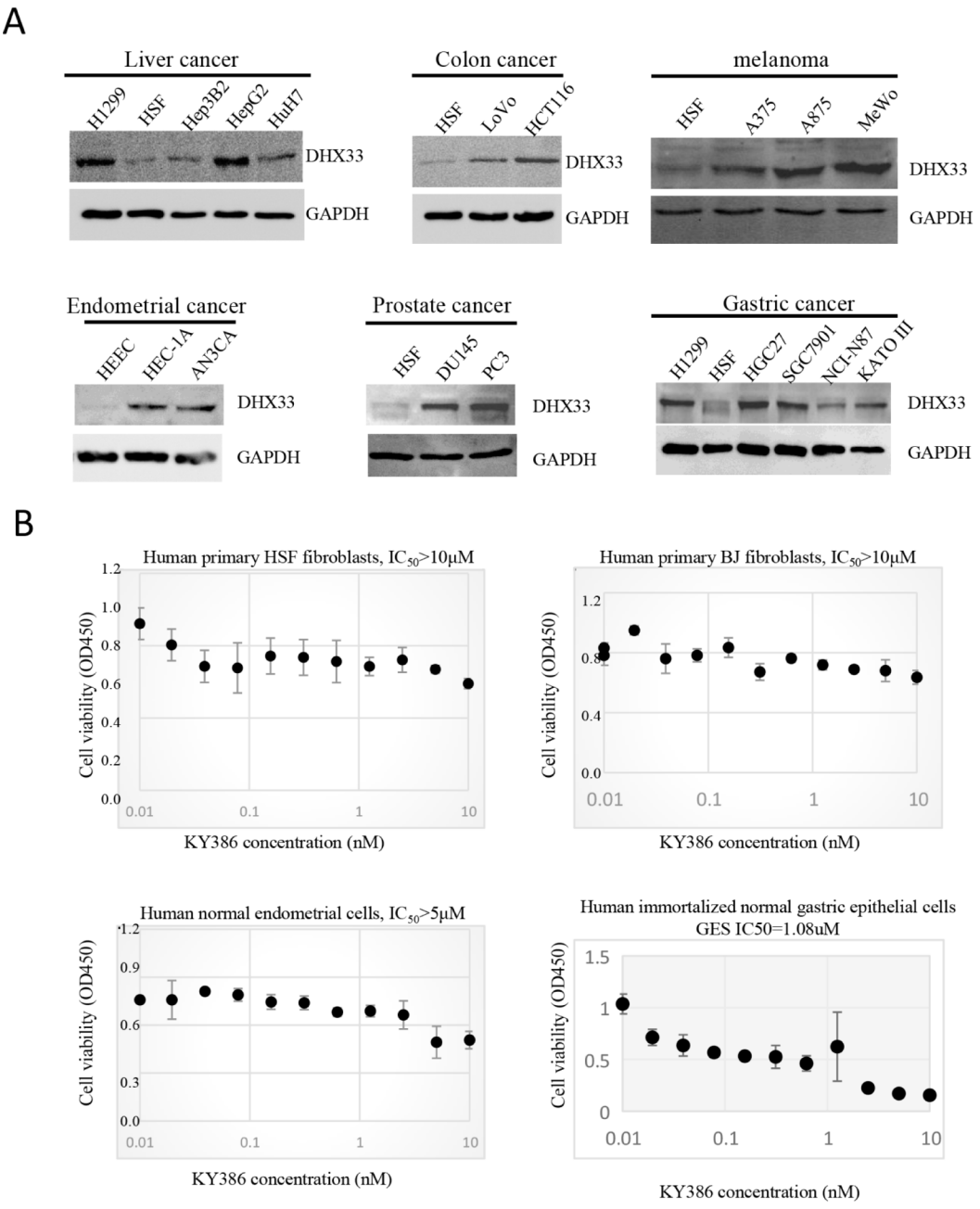

Figure 2. Normally differentiated cells and cancer cells with low DHX33 levels are less sensitive to KY386 inhibition. A. Different cancer cells with the same tissue origin were subjected to western blot analysis with the DHX33 antibody; GAPDH was used as an internal control. For controls, several human normal cells were also analyzed. B. CCK-8 analysis was performed on a few human normal cell lines for KY386 efficacy in vitro. Cells were treated at multiple doses for 72 h. The calculated IC_{50} was labeled in the graph.

RESULTS

KY386 Shows Broad Anticancer Activity. KY386 was previously developed by us to be a selective and potent inhibitor for DHX33 helicase.[27] However, no further experiments have been performed to evaluate its potential as a cancer therapeutic drug. In this study, the potential cytotoxicity effects of KY386 in 38 different types of cancer cell lines (including liver cancer, lung cancer, pancreatic cancer, colorectal cancer, gastric cancer, breast cancer, leukemia, renal cancer, prostate cancer, esophageal cancer, cervical cancer, brain cancer (glioblastoma) and melanoma) were analyzed. Cancer cell lines were treated at multiple doses for 72 h, and ATP content was measured and used as a surrogate of cell viability. Based on the results from the CellTiter-Glo analysis. KY386 appeared to exert an anticancer effect in most of these cancer cell lines, the half-maximum inhibitory concentration (IC_{50}) ranges from 24 nM to over 10 μM. Among these cell lines, the Capan-1 pancreatic cancer cell line, COLO 829 melanoma cancer cell line, SW480 colon cancer cell line, and Hep3B2 human liver cancer cell lines were less sensitive to the treatment of KY386. As shown in Figure 1A, KY386 demonstrated potent anticancer activity at nanomolar levels in many other cancer cell lines. Breast cancer cell lines with high DHX33 expression,[15] such as HCC1806, SK-BR-3 and BT549 cells, were sensitive to KY386 inhibition, with IC_{50} values in the range of 30−50 nM levels. Additionally, KY386 was effective in

https://doi.org/10.1021/acsomega.4c02265
ACS Omega 2024, 9, 28372−28384

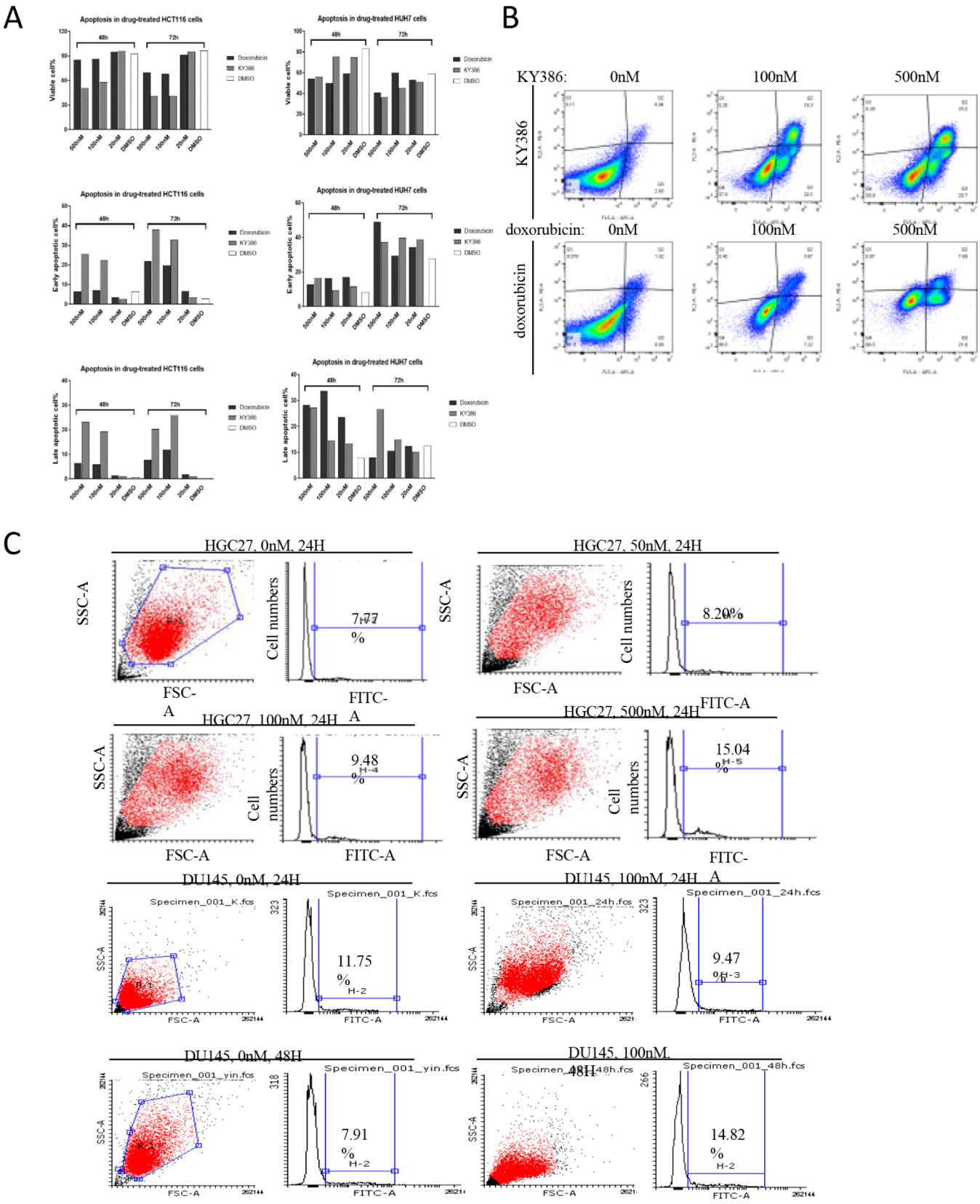

Figure 3. KY386 induced apoptosis in some cancer cells but much less efficient in others. A. Cell apoptosis analysis was performed in two representative cancer cell lines, HuH-7 and HCT116, and doxorubicin served as a positive control. KY386 was used at different concentrations. Cell apoptosis was analyzed based on Annexin V/PI staining from the standard protocol of Cell Vybrant kit. The apoptosis index was plotted. B. The dot plot for apoptosis analysis in (A). C.HGC27 and DU145 cells were treated with KY386 at different doses for the designated time points. Cell apoptosis analysis was then performed following the standard protocol of a Cell Vybrant kit. The apoptosis index was evaluated based on Annexin V staining only and was labeled on the graph.

https://doi.org/10.1021/acsomega.4c02265
ACS Omega 2024, 9, 28372−28384

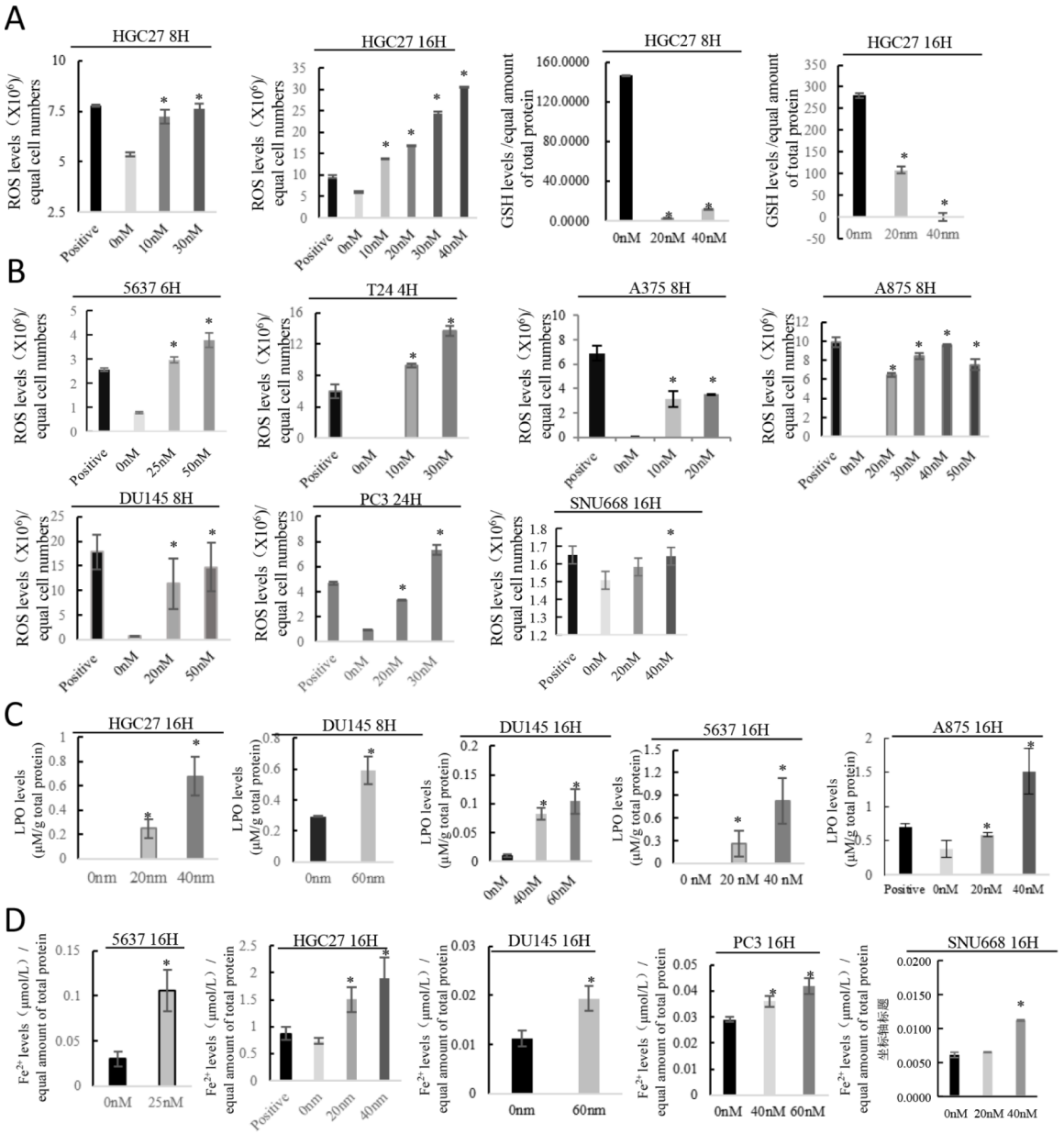

Figure 4. KY386 induced ferroptosis in a broad spectrum of cancer cells. A. HGC27 cells were treated with KY386 or inducer of ferroptosis (provided in the kit) at the indicated doses for either 8 or 16 h. Cells were then analyzed for ROS or GSH levels according to the standard protocol provided by the manufacture. Data reflected mean and standard deviation from three separate experiments. *, $p < 0.05$. B. Similarly, ROS levels were analyzed in other cancer cell lines after KY386 treatment for either 4, 6, 8 or 24 h. *, $p < 0.05$.C. Lipid peroxidation (LPO) levels were evaluated based on the standard protocol recommended by the manufacturer after cancer cells were treated with KY386 at different doses for the indicated time. *, $p < 0.05$. D. Fe^{2+} levels were evaluated based on the standard protocol recommended by the manufacturer after cancer cells were treated with KY386 at different doses for the indicated time. *, $p < 0.05$.

many RAS mutant cancer cell lines such as A549, H1299, H1975, and LOVO.

A few other cancer cell lines, A875, A375, T24, 5637, SGC7901, HGC27, and SNU668 cells were also utilized for the drug efficacy test through CCK-8 analysis, with Taxol for a comparison. The data are shown in Figure 1B. KY386 demonstrated good inhibition in all seven cancer cell lines. To analyze the effect of KY386 on cancer cell lines cultured in three-dimentional growth media, human cancer organoids were further used for a drug potency test. The pathological information of cancer patients can be found in Table S1. These organoids are mostly derived from late-stage human cancers with RAS mutation, after extensive chemotherapy or other precision medical treatment. As shown in Figure 1C, the DHX33 inhibitor also demonstrated a potent anticancer effect in 3-D cancer cultures. For metastatic lung cancer and metastatic pancreatic cancer with the RAS mutation, three organoids were chosen for each cancer type. Out of 6 human cancer organoids, we found that the DHX33 inhibitor demonstrated a potent inhibitory effect in four organoids at nanomolar levels.

Normally Differentiated Cells and Cancer Cells with Low DHX33 Levels Are Less Sensitive to KY386 Inhibition. To further evaluate the effect of KY386 on normal cells, we chose several normally differentiated cells for examination. Specifically, human primary fibroblasts HSF and

https://doi.org/10.1021/acsomega.4c02265
ACS Omega 2024, 9, 28372−28384

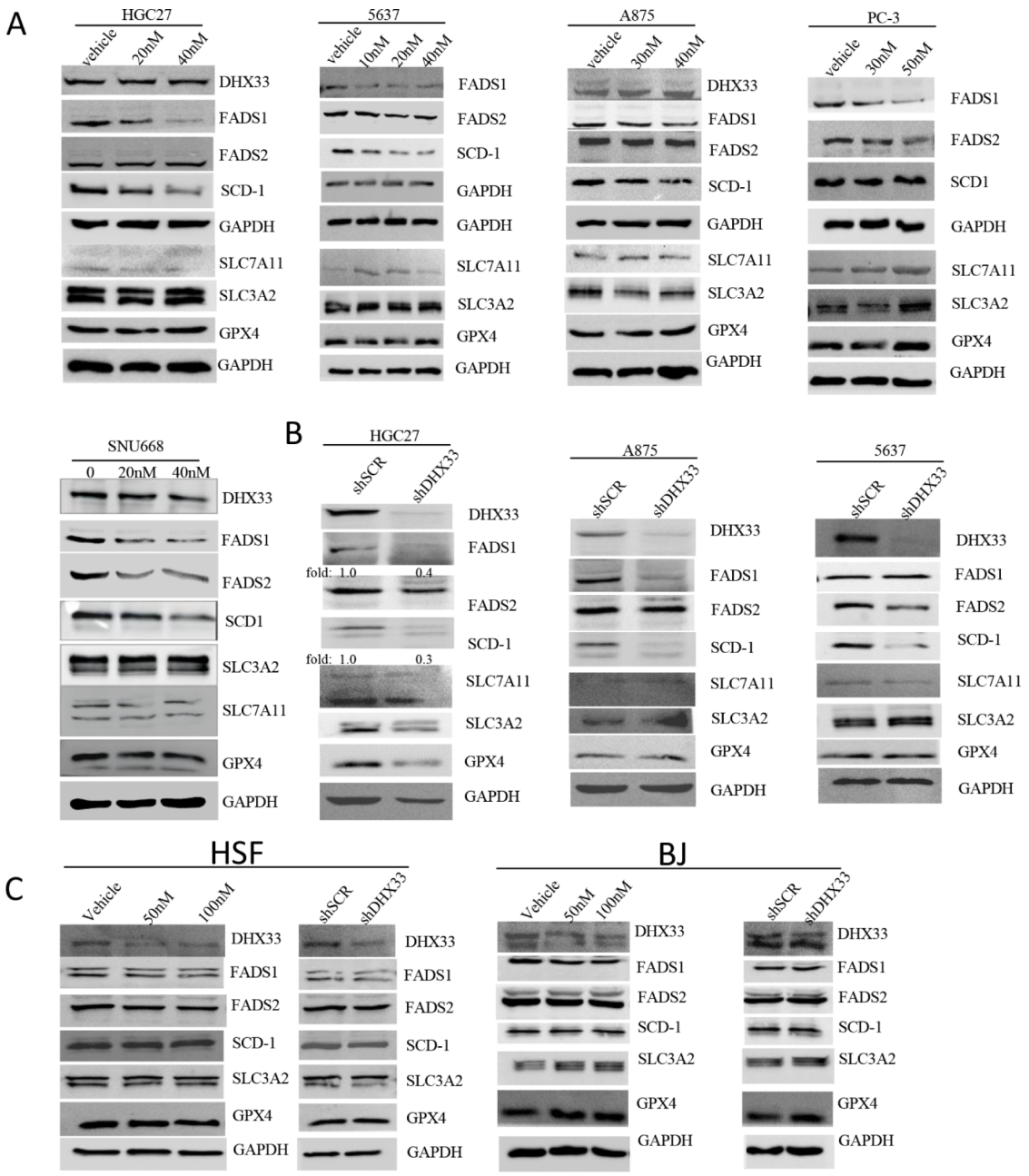

Figure 5. DHX33 promotes the expression of critical players in lipid metabolism including FADS1, FADS2 and SCD1. A. Cancer cells were treated with KY386 at the indicated doses for 24 h. Whole cell extracts were prepared and were subjected to western blot analysis with the indicated antibodies. GAPDH served as an internal control. B. Cancer cells were transduced by lentivirus to knockdown DHX33, and shScrambled (shSCR) was used as a control. Whole cell extracts were then analyzed by western blot with the indicated antibodies, and GAPDH serves as an internal control. C. Human normal cells HSF or BJ cells were either treated with KY386 at the indicated doses for 24 h, followed by whole cell lysates preparation, or were infected by lentivirus to knockdown DHX33, shScrambled was used as a control. Three days post infection, whole cell extracts were prepared. Western blot analysis was performed on these cell lysates with designated antibodies. GAPDH served as a control.

BJ, human normal endometrial HEEC cells, and immortalized human gastric epithelial GES cells were used for studies. First, the DHX33 protein expression levels were analyzed through western blotting, with GAPDH as a protein loading control. As shown in Figure 2A, both HSF and HEEC human normal cells showed lower expression of DHX33 protein as compared to the cancer cells with the same tissue origin. A drug efficacy test was then performed on these cell lines; as shown in Figure 2B, KY386 demonstrated little or limited efficacy in these normal cells. In HSF, BJ and HEEC cells, the IC_{50} values were identified to be over 10 μM, while in GES cells, IC_{50} was determined to be 1.08 μM. All of these IC_{50} values were significantly higher than those in many cancer cell lines. Notably, in a couple of cancer cell lines with low DHX33 expression, such as NCI-N87 and Hep3B2 cells, the IC_{50} values were between 1 and 2μM, too.

KY386 Induced Apoptosis in Some Cancer Cells but Not in Others. Decreased cell proliferation might be due to a reduction in cell proliferation or cell death. In order to differentiate between these two outcomes, cell apoptosis was first performed after the DHX33 inhibitor was applied. A DNA damaging agent, doxorubicin, served as a positive control. A

https://doi.org/10.1021/acsomega.4c02265
ACS Omega 2024, 9, 28372−28384

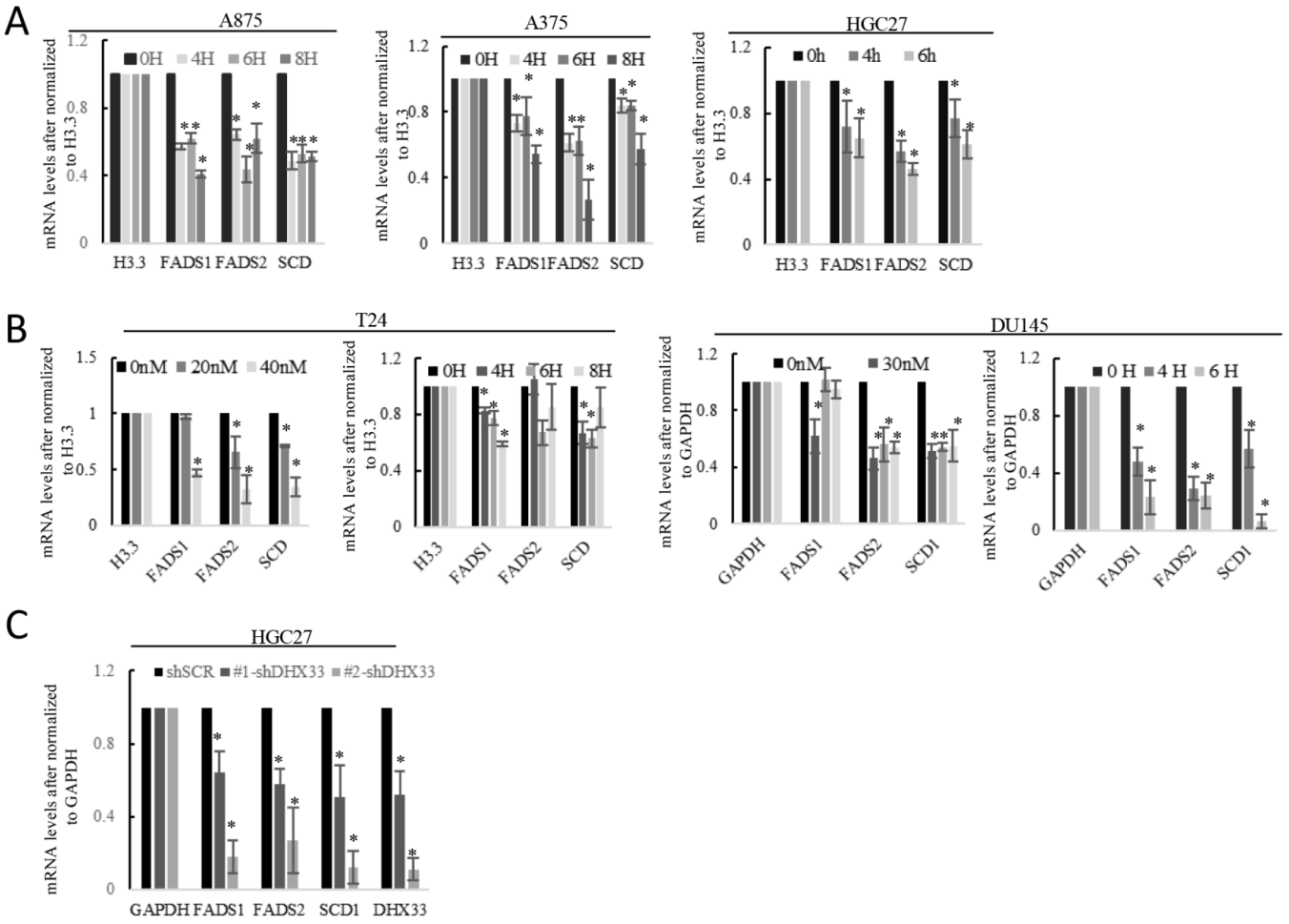

Figure 6. DHX33 regulates *fads1*, *fads2*, and *scd1* genes at the transcription level. A. A875, A375, and HGC27 cells were treated with KY386 at 40 nM for the indicated time points. Cells were then harvested, and total RNA was extracted for QPCR analysis with the indicated primer sets. Experiments were repeated at least twice, *, $p < 0.05$. B. T24 and DU145 cells were first treated with KY386 at the indicated doses for 6 h and then harvested for QPCR analysis. These cells were then analyzed for target gene expression after treatment with KY386 at 40 nM for the indicated time points. Total RNA was extracted for QPCR analysis. Experiments were repeated at least twice, *, $p < 0.05$. C. HGC27 cells were infected with lentivirus encoding either shSCR or shDHX33 to knockdown DHX33. 72 h postinfections, cells were harvested for total RNA extraction and QPCR analysis. Experiments were repeated at least twice, *, $p < 0.05$.

liver cancer cell line HuH7 and a RAS mutant colon cancer cell line HCT116 were used for analysis. As shown in Figure 3A,B, the DHX33 inhibitor potently induced apoptosis. Figure 3A shows the quantitation data for the apoptosis index, while Figure 3B shows the dot plot data. The apoptotic index increased in a dose-dependent manner and time-dependent manner. Though KY386 efficiently induced apoptosis in HuH7 and HCT116 cells, it did not cause a similar effect in a few other cancer cell lines that were analyzed. As shown in Figure 3C, both an increase in dose and an increase of KY386 treatment could not effectively induce apoptosis in the gastric cancer cell line HGC27 and prostate cancer cell line DU-145, though the drug efficacy test clearly demonstrated cell inhibition by KY386.

KY386 Induced Ferroptosis in a Broad Spectrum of Cancer Cells. From previous experimental results, cell death was clearly observed under the microscope, though not due to apoptosis. Ferroptosis has been previously reported to be induced by small molecule anticancer agents in cancer cells.[41,42] To further investigate the mechanism for how KY386 inhibited cancer cell proliferation, ferroptosis tests were performed. First, reactive oxygen species (ROS) levels were analyzed in cancer cells after KY386 treatment in HGC27 cells. HGC27 cells were treated with KY386 in different doses for either 8 or 16 h. ROS levels were then analyzed by fluoresecence based methods. As shown in Figure 4A, KY386 efficiently induced the ROS levels in cells in a time and dose dependent manner, as compared to the negative control. Concomitantly, glutathione (GSH) levels were reduced. The same phenomena were also observed in several other cancer cell lines analyzed, such as bladder cancer cell lines T24 and 5637, melanoma cell lines A375 and A875, prostate cancer cell lines DU145 and PC3, and SNU668 gastric cancer cells (Figure 4B). Other than ROS and GSH levels, the other hallmarks for ferroptosis, lipid peroxidation (LPO), and ferric ion (Fe^{2+}) were analyzed in KY386 treated cancer cells. As shown in Figure 4C, increased lipid peroxidation was observed in HGC27, 5637, DU145, SNU668, and A875 cells after KY386 treatment for 8 or 16 h. Ferric ions were also analyzed; as in ferroptosis, Fe^{2+} would accumulate to trigger lipid peroxidation in the lipid membrane. A dramatic increase of Fe^{2+} was observed in KY386 treated cells, as shown in Figure 4D.

https://doi.org/10.1021/acsomega.4c02265
ACS Omega 2024, 9, 28372−28384

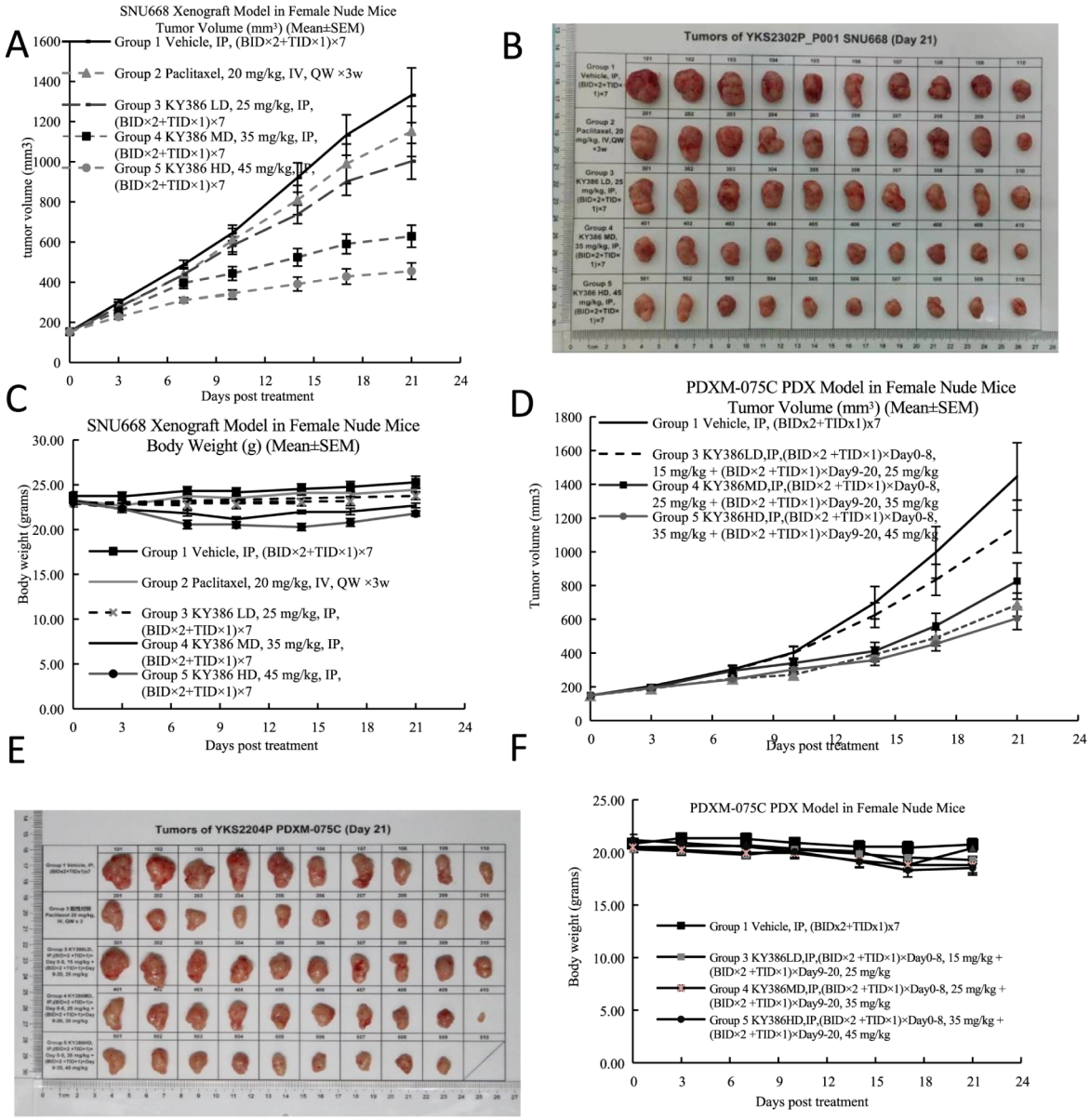

Figure 7. KY386 inhibits the growth of various human cancers in vivo. A. The SNU668 gastric xenograft model was set up, and mice were subjected to drug treatment through intraperitoneal injection. Tumor volume was monitored and calculated. B. Tumor images were taken after tumor dissection. C. Mouse body weight was monitored and plotted. D. Patient derived xenograft models for Ras G12D mutant colon cancers were set up and mice were subjected to drug treatment through intraperitoneal injection. Tumor volume was monitored and calculated. E. Tumor images were taken after tumor dissection. F. Mouse body weight was monitored and plotted.

DHX33 Promotes the Protein Expression of Critical Players in Lipid Metabolism Including FADS1, FADS2, and SCD1. Ferroptosis is tightly correlated to lipid metabolism, especially the polyunsaturated lipid (PUA) levels.[37] Evidence has shown that high PUA levels sensitize cancer cells to undergo ferroptosis.[43] To investigate the underlying molecular mechanism for KY386 to trigger ferroptosis, we analyzed a few genes that are related to ferroptosis were analyzed. Cancer cells were first treated with KY386 at different concentrations for 24 h. Whole cell lysates were then prepared and analyzed for proteins involved in ferroptosis; these proteins include FADS1, FADS2, SCD1, GPX4, SLC3A2, and SLC7A11, with GAPDH as an internal control. As shown in Figure 5A, at the protein level, KY386 treatment more preferentially caused the reduction of FADS and SCD1 expression, while it had a limited effect on GPX4, SLC3A2, and SLC7A11 expression. To confirm that KY386 indeed regulated these proteins via DHX33 but not due to an off-target effect, the same analysis was performed in DHX33 knockdown cells. DHX33 was knocked down through a lentiviral infection. Whole cell extracts were then analyzed for designated gene expression. As shown in Figure 5B, FADS and SCD1 expression was reduced at the protein levels after DHX33 knockdown, while those of GPX4, SLC3A2, and SLC7A11 were not influenced. Finally, the same analysis was performed in two normal human cell lines, HSF and BJ. Both KY386 treatment and DHX33 knockdown did not reduce the protein expression for FADS, SCD1, GPX4 and SLC3A2, and SLC7A11 (Figure 5C). These data indicate that KY386 more

https://doi.org/10.1021/acsomega.4c02265
ACS Omega 2024, 9, 28372−28384

preferentially kill cancer cells via ferroptosis but sparing normal cells.

To further investigate how DHX33 could regulate these genes, quantitative QPCR was performed on these cells after KY386 treatment. Significant downregulation of *fads1*, *fads2*, and *scd1* genes at the mRNA levels was observed. This occurred in a time- and dose dependent manner (Figure 6).

KY386 Inhibits the Growth of Various Human Cancers In Vivo. To analyze whether KY386 inhibits cancer growth in vivo, the cell line derived xenograft (CDX) mouse model was first analyzed. The SNU668 cell line has both RAS mutation and p53 mutation; this cancer model is hard to inhibit in vivo. Appropriate amounts of SNU668 cells were injected into the flanks of immunocompromised mice subcutaneously. When the tumors reached an average size of 150 mm^3 in volume, the mice were treated with KY386 or Taxol as a control through IP injection. The tumor size and mouse body weight were monitored at the indicated time point. Approximately 21 days later, KY386 was found to efficiently inhibit tumor growth in vivo, in a dose dependent manner, as shown by the tumor growth curves (Figure 7A) and tumor images (Figure 7B). Taxol could not marked inhibit tumor development in this model. Additionally, no marked toxicity was observed in the mice under KY386 treatment in this dosing regimen, as shown by no significant reduction of the body weights (Figure 7C). Next, a patient derived xenograft model, RAS G12D mutant colon cancer, was further evaluated for drug efficacy analysis. The pathological information for the patient is shown in Table S1. For this analysis, Taxol was also used as a control. Significant cancer inhibition for KY386 for RAS mutant colon cancer PDX (Figure 7D−F) was observed.

DISCUSSION

In this study, we provide evidence for a DHX33 inhibitor, KY386, to demonstrate its potent anticancer effect in a broad spectrum of cancer cells. We further unveil a novel molecular mechanism for KY386 to inhibit cancer cell proliferation via sensitization of ferroptosis. Our results support the notion that DHX33 protein can be explored as a novel therapeutic target for treating human cancers, especially with RAS mutation. This DHX33 inhibitor KY386 more preferentially kill cancer cells than normal cells with little toxicity in vivo.

Drug efficacy tests in over 40 different cancer cell lines reveal that KY386 has broad anticancer activity with selectivity. In the breast cancer cell panel, KY386 shows higher potency (IC_{50} ~ 30 nM to 50 nM) against cell lines with higher DHX33 protein expression, but shows lower potency (IC_{50} ~ 86 to100 nM) for MDA-MB-231 cells with lower DHX33 expression.[15] Additionally, in the lung cancer cell panel, DHX33 highly expressing H1299 and A549 cells are more sensitive to KY386 treatment than Calu-1 cells with lower DHX33 protein levels.[24,44] Hep3B2 has a low DHX33 protein level and is less sensitive to KY386 treatment. Similarly, NCI-N87 cells also have low expression of DHX33 protein, and it is less sensitive to KY386 treatment. Human normal cells have low expression of DHX33, and their IC_{50} values for KY386 are over than 1 μM. These data support the conclusion that KY386 has broad anticancer activity toward various cancer types. At least in a subset of breast cancer, colon cancer, and liver cancer cell lines, KY386 exhibited higher potency for DHX33 overexpressing cancer cells.

KY386 has a novel mechanism to kill cancer cells other than apoptosis. Increased ROS levels can be detected as early as 4 h post KY386 treatment in cancer cells (data not shown). Soon after KY386 treatment, cell death can be observed, as manifested by cell detachment, roundup, and death. The increase in ROS is accompanied by reduced GSH levels and increased LPO and ferric ion accumulation. All of these adhere to the ferroptosis hallmarks of cancer cell. The underlying molecular mechanism appears to be associated with the altered PUA metabolism in cancer cells. DHX33 drives the expression of FADS (especially FADS1) and SCD1 expression. Elevation of PUA in cells, in turn, sensitizes cancer cells to undergo ferroptosis after KY386 treatment. In contrast, the other critical players in ferroptosis, including GPX4, SLC3A2, and SLC7A11, were not found to be altered markedly. We propose that this occurs in a wide variety of cancer cells.

Notably, in both HGC27 and DU-145 cells, KY386 was found to induce apoptosis less efficiently and usually at later time points. Data showed that a small percentage of apoptosis can be detected at 48 h post KY386 treatment in HGC27 cells. Apoptosis in DU-145 was even less efficient after KY386 treatment (data not shown). As no apoptosis could be detected at 24 h post treatment, there is a possibility that apoptosis could be due to secondary responses by KY386. The different outcome might result from the different genetic background or cellular context, especially the different lipid metabolism and FADS1/SCD1 protein levels. Cancer cells have different rates of lipid metabolism; thus, they have different responses to KY386 treatment. Cancer cells with higher DHX33 and FADS1/SCD1 protein levels are more susceptible to ferroptosis after KY386 treatment. Higher DHX33 and FADS1/SCD1 protein levels could potentially serve as ferroptosis markers by KY386 treatment.

DHX33 protein has been found to be highly expressed in many human cancer, including liver cancer, colon cancer, glioblastoma, lymphoma, and pancreatic cancer, among others.[16,19,21,22] Though the RNA helicase family is regarded as RNA binding proteins, DHX33 has been found to primarily localize to the cell nuclei and bind to DNA elements in the GC rich regions.[24] DHX33 associates with transcription factor AP-2β in a subset of gene promoters and promote DNA demethylation via recruiting DNA demethylation proteins such as Gadd45a and Tet1.[24] Many genes were influenced at the transcriptional levels after DHX33 knockdown in various human cancer cells,[15,16,20,23,24,26,44] The underlying mechanism is generally associated with the DNA demethylation on gene promoters and thereby the impact on the initiation of transcription initiation. Hundreds of genes were influenced after DHX33 knockdown, and there is a global change in the transcriptome in human cancer cell lines. The influenced genes are involved in multiple cellular pathways, such as cell cycle progression, tumor metabolism, cytokinesis, chromosome remodeling, etc.[15,16,20,23,24,26,44] Many of these genes play pivotal roles in tumor development. We also provide the RNA sequencing result after DHX33 inhibition in A875 cells to demonstrate the transcriptome change, as shown in Table S2. Given the important roles of DHX33 in cancer development, this field holds promise for therapeutic values for developing novel anticancer drugs in future.

Given that little attention has been paid to RNA helicases in general over the past years with regard to their potential of therapeutic value, we certainly hope more and more attention should be paid to the RNA helicase family, and we fully

https://doi.org/10.1021/acsomega.4c02265
ACS Omega 2024, 9, 28372−28384

support further and extensive studies for these proteins, as they are the hub of RNA metabolism.

■ ASSOCIATED CONTENT

Supporting Information

The Supporting Information is available free of charge at https://pubs.acs.org/doi/10.1021/acsomega.4c02265.

Pathological information of cancer patients (PDF)

RNA sequencing result after DHX33 inhibition in A875 cells (PDF)

■ AUTHOR INFORMATION

Corresponding Author

Yandong Zhang − *Shenzhen KeYe Life Technologies Co., Ltd, Shenzhen, Guangdong 518155, China;* orcid.org/0009-0005-3811-8586; Phone: 86-755-21031732; Email: zhangyd@keye-life.com

Authors

Xiyu Tang − *Shenzhen KeYe Life Technologies Co., Ltd, Shenzhen, Guangdong 518155, China*

Yuanlian Deng − *Shenzhen KeYe Life Technologies Co., Ltd, Shenzhen, Guangdong 518155, China*

Yingying Liang − *Shenzhen KeYe Life Technologies Co., Ltd, Shenzhen, Guangdong 518155, China*

Deqing Liao − *Shenzhen KeYe Life Technologies Co., Ltd, Shenzhen, Guangdong 518155, China*

Fuyu Wen − *Shenzhen KeYe Life Technologies Co., Ltd, Shenzhen, Guangdong 518155, China*

Complete contact information is available at: https://pubs.acs.org/10.1021/acsomega.4c02265

Author Contributions

#X.Y., Y.D., and Y.L. contributed equally to this work

Funding

This work was supported by funds from Shenzhen KeYe Life Technologies Co., Ltd.

Notes

The authors declare no competing financial interest.

■ ACKNOWLEDGMENTS

We show our gratitude for Xianglu Li who gave great encouragement and help in raising funds for this drug development project.

■ REFERENCES

(1) Pyle, A. M. Translocation and unwinding mechanisms of RNA and DNA helicases. *Annu. Rev. Biophys.* **2008**, *37*, 317−336.

(2) Umate, P.; Tuteja, N.; Tuteja, R. Genome-wide comprehensive analysis of human helicases. *Commun. Integr Biol.* **2011**, *4* (1), 118−137.

(3) Tanner, N. K.; Linder, P. DExD/H box RNA helicases: From generic motors to specific dissociation functions. *Mol. Cell.* **2001**, *8* (2), 251−262.

(4) Aubourg, S.; Kreis, M.; Lecharny, A. The DEAD box RNA helicase family in Arabidopsis thaliana. *Nucleic Acids Res.* **1999**, *27* (2), 628−636.

(5) Donsbach, P.; Klostermeier, D. Regulation of RNA helicase activity: Principles and examples. *Biol. Chem.* **2021**, *402* (5), 529−559.

(6) Bohnsack, K. E.; Yi, S.; Venus, S.; Jankowsky, E.; Bohnsack, M. T. Cellular functions of eukaryotic RNA helicases and their links to human diseases. *Nat. Rev. Mol. Cell Biol.* **2023**, *24* (10), 749−769.

(7) Sloan, K. E.; Bohnsack, M. T. Unravelling the Mechanisms of RNA Helicase Regulation. *Trends Biochem. Sci.* **2018**, *43* (4), 237−250.

(8) Venus, S.; Jankowsky, E. Measuring the impact of cofactors on RNA helicase activities. *Methods* **2022**, *204*, 376−385.

(9) Cordin, O.; Banroques, J.; Tanner, N. K.; Linder, P. The DEAD-box protein family of RNA helicases. *Gene* **2006**, *367*, 17−37.

(10) Linder, P.; Jankowsky, E. From unwinding to clamping - the DEAD box RNA helicase family. *Nat. Rev. Mol. Cell Biol.* **2011**, *12* (8), 505−516.

(11) Bleichert, F.; Baserga, S. J. The long unwinding road of RNA helicases. *Mol. Cell.* **2007**, *27* (3), 339−352.

(12) Zhang, L.; Li, X. DEAD-Box RNA Helicases in Cell Cycle Control and Clinical Therapy. *Cells* **2021**, *10* (6), 1540.

(13) Fuller-Pace, F. V. DEAD box RNA helicase functions in cancer. *RNA Biol.* **2013**, *10* (1), 121−132.

(14) Wang, X.; Ge, W.; Zhang, Y. Recombinant DHX33 Protein Possesses Dual DNA/RNA Helicase Activity. *Biochemistry* **2019**, *58* (4), 250−258.

(15) Wang, J.; Feng, W.; Yuan, Z.; Weber, J. D.; Zhang, Y. DHX33 Interacts with AP-2β To Regulate Bcl-2 Gene Expression and Promote Cancer Cell Survival. *Mol. Cell. Biol.* **2019**, *39*, No. e00017.

(16) Fu, J.; Liu, Y.; Wang, X.; Yuan, B.; Zhang, Y. Role of DHX33 in c-Myc-induced cancers. *Carcinogenesis* **2017**, *38* (6), 649−660.

(17) Mitoma, H.; Hanabuchi, S.; Kim, T.; Bao, M.; Zhang, Z.; Sugimoto, N.; et al. The DHX33 RNA helicase senses cytosolic RNA and activates the NLRP3 inflammasome. *Immunity* **2013**, *39* (1), 123−135.

(18) Liu, Y.; Lu, N.; Yuan, B.; Weng, L.; Wang, F.; Liu, Y. J.; et al. The interaction between the helicase DHX33 and IPS-1 as a novel pathway to sense double-stranded RNA and RNA viruses in myeloid dendritic cells. *Cell. Mol. Immunol.* **2014**, *11* (1), 49−57.

(19) Zhu, Y.; Du, Y.; Zhang, Y. DHX33 promotes colon cancer development downstream of Wnt signaling. *Gene* **2020**, *735*, 144402.

(20) Wang, X.; Feng, W.; Peng, C.; Chen, S.; Ji, H.; Zhong, H.; et al. Targeting RNA helicase DHX33 blocks Ras-driven lung tumorigenesis in vivo. *Cancer Sci.* **2020**, *111* (10), 3564−3575.

(21) Tian, Q. H.; Zhang, M. F.; Luo, R. G.; Fu, J.; He, C.; Hu, G.; et al. DHX33 expression is increased in hepatocellular carcinoma and indicates poor prognosis. *Biochem. Biophys. Res. Commun.* **2016**, *473* (4), 1163−1169.

(22) Wang, H.; Yu, J.; Wang, X.; Zhang, Y. The RNA helicase DHX33 is required for cancer cell proliferation in human glioblastoma and confers resistance to PI3K/mTOR inhibition. *Cell. Signal.* **2019**, *54*, 170−178.

(23) Peng, C.; Hou, S. T.; Deng, C. X.; Zhang, Y. Function of DHX33 in promoting Warburg effect via regulation of glycolytic genes. *J. Cell. Physiol.* **2021**, *236* (2), 981−996.

(24) Yuan, B.; Wang, X.; Fan, C.; You, J.; Liu, Y.; Weber, J. D.; et al. DHX33 Transcriptionally Controls Genes Involved in the Cell Cycle. *Mol. Cell. Biol.* **2016**, *36* (23), 2903−2917.

(25) Fraile, J. M.; Campos-Iglesias, D.; Rodríguez, F.; Astudillo, A.; Vilarrasa-Blasi, R.; Verdaguer-Dot, N.; et al. Loss of the deubiquitinase USP36 destabilizes the RNA helicase DHX33 and causes preimplantation lethality in mice. *J. Biol. Chem.* **2018**, *293* (6), 2183−2194.

(26) Wang, X.; Chen, S.; Wen, F.; Zeng, Y.; Zhang, Y. RNA helicase DHX33 regulates HMGB family genes in human cancer cells. *Cell. Signal.* **2023**, *110*, 110832.

(27) Wang, Y.; Nie, G.; Wang, X.; Ge, W.; Zhang, Y. Development of small molecule inhibitors targeting RNA helicase DHX33 as anti-cancer agents. *Bioorg. Med. Chem. Lett.* **2023**, *96*, 129505.

(28) Dixon, S. J.; Lemberg, K. M.; Lamprecht, M. R.; Skouta, R.; Zaitsev, E. M.; Gleason, C. E.; et al. Ferroptosis: an iron-dependent form of nonapoptotic cell death. *Cell* **2012**, *149* (5), 1060−1072.

(29) Park, E.; Chung, S. W. ROS-mediated autophagy increases intracellular iron levels and ferroptosis by ferritin and transferrin receptor regulation. *Cell Death Dis.* **2019**, *10* (11), 822.

(30) Zhong, F. M.; Yao, F. Y.; Liu, J.; Zhang, H. B.; Zhang, J.; Zhang, N.; et al. Ferroptosis-related molecular patterns reveal immune escape, inflammatory development and lipid metabolism characteristics of the tumor microenvironment in acute myeloid leukemia. *Front. Oncol.* **2022**, *12*, 888570.
(31) Yang, W. S.; Kim, K. J.; Gaschler, M. M.; Patel, M.; Shchepinov, M. S.; Stockwell, B. R. Peroxidation of polyunsaturated fatty acids by lipoxygenases drives ferroptosis. *Proc. Natl. Acad. Sci. U. S. A.* **2016**, *113* (34), No. E4966.
(32) Liu, H.; Deng, Z.; Yu, B.; Liu, H.; Yang, Z.; Zeng, A.; Fu, M. Identification of SLC3A2 as a Potential Therapeutic Target of Osteoarthritis Involved in Ferroptosis by Integrating Bioinformatics, Clinical Factors and Experiments. *Cells* **2022**, *11* (21), 3430.
(33) Liu, M. R.; Zhu, W. T.; Pei, D. S. System Xc(−): A key regulatory target of ferroptosis in cancer. *Invest. New Drugs.* **2021**, *39* (4), 1123−1131.
(34) Xu, T.; Ding, W.; Ji, X.; Ao, X.; Liu, Y.; Yu, W.; et al. Molecular mechanisms of ferroptosis and its role in cancer therapy. *J. Cell. Mol. Med.* **2019**, *23* (8), 4900−4912.
(35) Yano, K. Lipid metabolic pathways as lung cancer therapeutic targets: a computational study. *Int. J. Mol. Med.* **2012**, *29* (4), 519−529.
(36) Tesfay, L.; Paul, B. T.; Konstorum, A.; Deng, Z.; Cox, A. O.; Lee, J.; et al. Stearoyl-CoA Desaturase 1 Protects Ovarian Cancer Cells from Ferroptotic Cell Death. *Cancer Res.* **2019**, *79* (20), 5355−5366.
(37) Lee, J. Y.; Nam, M.; Son, H. Y.; Hyun, K.; Jang, S. Y.; Kim, J. W.; et al. Polyunsaturated fatty acid biosynthesis pathway determines ferroptosis sensitivity in gastric cancer. *Proc. Natl. Acad. Sci. U. S. A.* **2020**, *117* (51), 32433−32442.
(38) Wang, R.; Zhang, J.; Ren, H.; Qi, S.; Xie, L.; Xie, H.; Shang, Z.; Liu, C. Dysregulated palmitic acid metabolism promotes the formation of renal calcium-oxalate stones through ferroptosis induced by polyunsaturated fatty acids/phosphatidic acid. *Cell. Mol. Life Sci.* **2024**, *81* (1), 85.
(39) Zhang, Y.; Forys, J. T.; Miceli, A. P.; Gwinn, A. S.; Weber, J. D. Identification of DHX33 as a mediator of rRNA synthesis and cell growth. *Mol. Cell. Biol.* **2011**, *31* (23), 4676−4691.
(40) Zhang, Y.; You, J.; Wang, X.; Weber, J. The DHX33 RNA Helicase Promotes mRNA Translation Initiation. *Mol. Cell. Biol.* **2015**, *35* (17), 2918−2931.
(41) Lachaier, E.; Louandre, C.; Godin, C.; Saidak, Z.; Baert, M.; Diouf, M.; Chauffert, B.; Galmiche, A. Sorafenib induces ferroptosis in human cancer cell lines originating from different solid tumors. *Anticancer Res.* **2014**, *34* (11), 6417−6422.
(42) Ooko, E.; Saeed, M. E.; Kadioglu, O.; Sarvi, S.; Colak, M.; Elmasaoudi, K.; et al. Artemisinin derivatives induce iron-dependent cell death (ferroptosis) in tumor cells. *Phytomedicine* **2015**, *22* (11), 1045−1054.
(43) Kim, M. J.; Yun, G. J.; Kim, S. E. Metabolic Regulation of Ferroptosis in Cancer. *Biology* **2021**, *10* (2), 83.
(44) Nie, G.; Chen, S.; Song, Q.; Zou, D.; Li, M.; Tang, X.; et al. DHX33 mediates p53 to regulate mevalonate pathway gene transcription in human cancers. *Biochim. Biophys. Acta, Gen. Subj.* **2024**, *1868* (3), 130547.

https://doi.org/10.1021/acsomega.4c02265
ACS Omega 2024, 9, 28372−28384